PCCP

Accepted Manuscript

ROYAL SOCIETY OF CHEMISTRY

www.rsc.org/pccp

ARTICLE TYPE www. rsc.org/xxxxxx | XXXXXXXX

Energy level alignment in TiO_2/metal sulfide/polymer interfaces for solar cell applications

Rebecka Lindblad,[a] Ute Cappel,[b] Flannan T. F. O'Mahony,[b] Hans Siegbahn,[a] Erik M. J. Johansson,[c] Saif A. Haque,*[b] and Håkan Rensmo*[a]

Received Xth XXXXXXXXXX 20XX, Accepted Xth XXXXXXXXX 20XX
First published on the web Xth XXXXXXXXXX 200X
DOI: 10.1039/b000000x

Semiconductor sensitized solar cell interfaces have been studied with photoelectron spectroscopy to understand the interfacial electronic structures. In particular, the experimental energy level alignment has been determined for complete TiO_2/metal sulfide/polymer interfaces. For the metal sulfides CdS, Sb_2S_3 and Bi_2S_3 deposited from single source metal xhanthate precursors, it was shown that both driving forces for electron injection into TiO_2 and hole transfer to the polymer decrease for narrower bandgaps. The energy level alignment results was used in the discussion of the function of solar cells with the same metal sulfides as light absorbers. For example Sb_2S_3 showed the most favourable energy level alignment with 0.3 eV driving force for electron injection and 0.4 eV driving force for hole transfer and also the most efficient solar cells due to high photocurrent generation. The energy level alignment of the TiO_2/Bi_2S_3 interface on the other hand showed no driving force for electron injection to TiO_2, and the performance of the corresponding solar cell was very low.

1 Introduction

Semiconductor sensitized solar cells are promising devices for conversion of solar energy to electricity[1]. These solar cells derive their architecture from dye-sensitized solar cells[2,3] but use a small bandgap semiconductor to sensitize a substrate of a mesoporous semiconductor (TiO_2), instead of dye molecules typically employed in dye-sensitized solar cells. The small bandgap semiconductor absorbs visible light and the charge separation occurs at the interfaces between the TiO_2, the absorber and a hole conductor.

Solution-processable nanocrystalline metal chalcogenides are candidates as light absorbers in this type of solar cell, for example Sb_2S_3[4–7], CdS[8] and PbS[9,10] of which Sb_2S_3 has been the most successful. Sb_2S_3 has been used in combination with different solid state hole conductors, and record power conversion efficiencies of 5% and 7.5% have been achieved when using the polymers poly-3-hexylthiophene (P3HT)[5] and (poly(2,6-(4,4-bis-(2-ethylhexyl)- 4H-cyclopenta[2,1-b;3,4-b']dithiophene)-alt-4,7(2,1,3-benzothiadiazole)) (PCPDTBT)[11], respectively.

Understanding of the interfacial electronic and chemical structures are important for the design of efficient solar cells. For example, to facilitate charge separation and to obtain an efficiently working solar cell, a favourable energy level alignment at the different interfaces is required. Valence band edges extracted from various types of measurements can be found in the literature; UV photoelectron spectroscopy (UPS), flat band potential measurements and cyclic voltammetry are some examples[3,12–14]. Typically, the valence band edge of the bulk materials are used when comparing the energy levels at interfaces[15,16]. Valence band edges measured with different methods are sometimes also compared[17,18]. To study the different materials in similar conditions using one method has advantages for a reliable energy level alignment. Ideally, the materials should even be studied simultaneously, in particular material combinations, since it is probable that the energy level alignment is affected when two materials are brought in contact to each other[19].

Even though UPS is a common method to study valence band offsets of various metal sulfides, semiconductors and polymers[15,20], the surface sensitivity of UPS excludes measurements of a buried material. When using higher photon energies (as in X-ray based photoelectron spectroscopy, PES, or hard X-ray photoelectron spectroscopy, HAXPES) it becomes possible to study a complete interface and in this way directly relate the energy levels in the substrate and the adsorbed material[21–23]. Here, we show that the complete semiconductor/light-absorber/hole conductor interface can be measured with soft X-ray photoelectron spectroscopy. In a single experiment, it is therefore possible to relate energy lev-

[a] *Department of Physics and Astronomy, Molecular and Condensed Matter Physics, Uppsala University, Box 516, SE-751 20 Uppsala, Sweden. E-mail: hakan.rensmo@physics.uu.se*
[b] *Centre for Plastic Electronics, Department of Chemistry, Imperial College London, South Kensington Campus, Exhibition Road, SW7 2AZ, U.K. E-mail: s.a.haque@imperial.ac.uk*
[c] *Department of Chemistry, Ångström, Uppsala University, Box 259, SE-751 05 Uppsala, Sweden.*

els in both a light-absorber and a polymer to energy levels in the substrate. We compare measurements of the electronic core levels with the valence bands and relate the position of the valence band edges of the different materials. The results obtained from the photoelectron spectroscopy measurements are then related to the function of solar cells based on the same metal sulfides. The same method can be applied to other active interfaces such as those found in hybrid solar cells[24] and dye-sensitized solar cells[25], where the interface structure is highly related to the function of the device.

We have included the three metal sufides, CdS, Sb_2S_3 and Bi_2S_3 in this study, in order to compare two materials which work in solar cells (CdS and Sb_2S_3) to a material, which has not been successfully used to sensitize TiO_2 (Bi_2S_3). For Sb_2S_3, we compare the energy alignment to P3HT and PCPDTBT, the two most successful hole conductors so far (see figure 1 for molecular structures).

To find useful deposition techniques is important for manufacturing of solar cells. In this investigation the metal sulfides were deposited on the TiO_2 surface from single source metal xanthate precursors (chemical structures are found in figure 1), which were converted to metal sufides through annealing under nitrogen[26]. Xanthate precursors have recently been used to make hybrid solar cells with blends of sulfides and polymers as active layers[27–29] and to deposit mesoporous films of antimony sulfide where the sulfide acts as both light absorber and electron transporting material[30]. The method can be adapted to deposit different sulfides on mesoporous TiO_2 surfaces without the need for lengthy optimization, which may be required in more conventional deposition methods such as chemical bath deposition and successive ionic layer deposition.

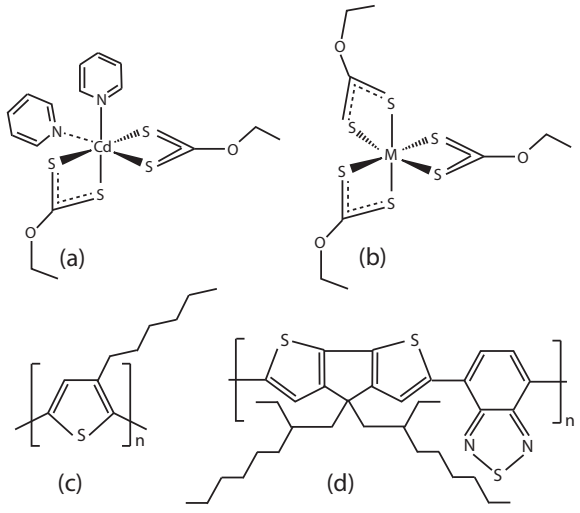

Fig. 1 Molecular structures of (a) Cd xanthate (b) Sb and Bi xanthate (where M is Sb or Bi) (c) P3HT and (d) PCPDTBT.

2 Experimental section

Both solar cell samples and PES samples were fabricated on ITO substrates. For solar cells, a dense TiO_2 was deposited by spincoating a solution of titanium isopropoxide (97%, Sigma Aldrich) and ethanolamine in 2-methoxyethanol. Following this, a mesoporous TiO_2 layer was fabricated by spinning a TiO_2 paste (Dyesol, 18NRT), which had been diluted with terpineol in a 1:2 ratio. For PES samples, this paste was spun directly onto the ITO substrates. All films were then sintered at 450° C for 30 minutes with resulting film thicknesses of approximately 250 nm. A titanium tetrachloride treatment was then carried out by immersing the films in a 20 mM solution of titanium(IV) chloride tetrahydrofuran (Aldrich) in water at 70° C for 30 minutes. Films were rinsed in water and isopropanol following this treatment and then sintered again at 450° C. Cadmium, antimony and bismuth xanthate were synthesised as described in literature[26]. The concentration and spincoating speed can be varied to obtain thicknesses that allow for PES analysis as well as solar cell function. For PES samples 400 mg/ml solutions in chlorobenzene of all three xanthates were prepared and deposited on top of the TiO_2 films by spincoating either at 2000 rpm (Sb_2S_3) or 5000 rpm (CdS and Bi_2S_3). For solar cells, 300 mg/ml solutions of bismuth and cadmium xanthate were used and all precursors were spun at 2000 rpm. Sulfide formation was induced by annealing at 160° C for cadmium and bismuth and at 300° C for antimony in a nitrogen filled glove box. Where applicable for PES samples, regioregular P3HT (Mn 54,000-75,000, Plextronics) or PCPDTBT (average Mw 7,000-20,000, Aldrich) were deposited by spincoating from a 12.5 mg/ml solution in chlorobenzene at 10000 rpm (P3HT) or at 4000 rpm (PCPDTBT). P3HT was spun at 2000 rpm from a 12.5 mg/ml solution for solar cells and device fabrication was completed by evaporating a 100 nm thick silver back contact. PCPDTBT was deposited from a 15 mg/ml solution with 2000 rpm for a TiO_2/Sb_2S_3 solar cell.

Samples studied with PES were mesoporous TiO_2, mesoporous TiO_2 covered with a metal sulfide (TiO_2/CdS, TiO_2/Sb_2S_3, TiO_2/Bi_2S_3) and mesoporous TiO_2 covered with first a metal sulfide and then a polymer (TiO_2/Sb_2S_3/P3HT, TiO_2/Sb_2S_3/PCPDTBT). Films of the polymers spin coated on ITO (ITO/P3HT and ITO/PCPDTBT) were also studied for comparison.

Photoelectron spectroscopy was performed at beamline I411[31] at the MAX IV laboratory in Lund in Sweden. All spectra are binding energy calibrated versus the Fermi level at zero binding energy measured on a TiO_2 sample. The other samples are aligned using TiO_2 core levels. The experimental broadening (FWHM) is below 0.1 eV for the valence level measurements and 0.3 eV for the core level measurements. The uncertainty of the binding energy calibration is estimated

to be smaller than 0.05 eV. The thicker polymer films deposited on ITO do not contain TiO_2 and therefore these measurements are compared to the TiO_2/metal sulfide/polymer samples by aligning the signal from the S 2p core level originating from the polymer. If not stated otherwise, the intensity of the spectra are scaled so that the most intense peaks have the same height.

Solar cells were characterised by measuring IV-curves using a 150 W Xenon lamp (ScienceTech SS150W solar simulator) equipped with an AM1.5 filter (ScienceTech) and an IR filter (Water Filter) as irradiation source and a Keithley 2400 series source meter to measure the current. IPCE spectra were measured using irradiation from a quartz halogen lamp (Bentham IL1) filtered through a monochromator (Bentham M300) and a Keithley 2400 series source meter.

UV-visible absorption measurements were carried out on a Shimadzu UV-2600 equipped with an integrating sphere. Both transmittance (T) and reflectance (R) were measured and the absorptance was calculated according to the formula:

$$Absorptance = 1 - T - R. \quad (1)$$

3 Results and discussion

3.1 Absorption spectra

Absorption spectra of the different sulfides deposited onto TiO_2 measured on a UV-visible spectrometer equipped with an integrating sphere are shown in figure 2. It can be seen that going from CdS to Sb_2S_3 increasingly large portions of the visible (and near-infrared) spectrum are being absorbed. Absorption spectra of the polymers, regioregular P3HT and PCPDTBT, which were used in this study, are also included in figure 2. The onsets of the absorbtance can be compared to the bandgap of the materials. Bandgap values found in the literature are 2.4 for CdS[8,14], 1.7–1.8 eV for Sb_2S_3[14,32,33], 1.1–1.6 eV for Bi_2S_3[33,34], 1.9 eV for P3HT[35,36] and 1.4–1.59 eV for PCPDTBT[37,38]. We use these values (or the average of the reported values) to estimate the absorption onsets: 510 nm for CdS, 740 nm for Sb_2S_3, 950 nm for Bi_2S_3, 650 nm for P3HT and 840 for PCPDTBT. These calculated onsets are marked in figure 2 and are in good agreement with results from the absorbtance spectra. The absence of discrete absorption peaks for the metal sulfides indicates a distribution of particle sizes, or a continuous film, without quantum confinement effects[26].

3.2 Photoelectron spectroscopy characterization

3.2.1 TiO_2/metal sulfide interfaces. Figure 3 shows overview spectra of mesoporous TiO_2 before and after the introduction of the different metal sulfides. Titanium and oxygen from the TiO_2 substrate is visible in all samples. Some carbon is also seen in all samples, which is expected as contamination on *ex situ* samples. Otherwise the metal sulfide samples only contain the corresponding metal and sulfur core levels.

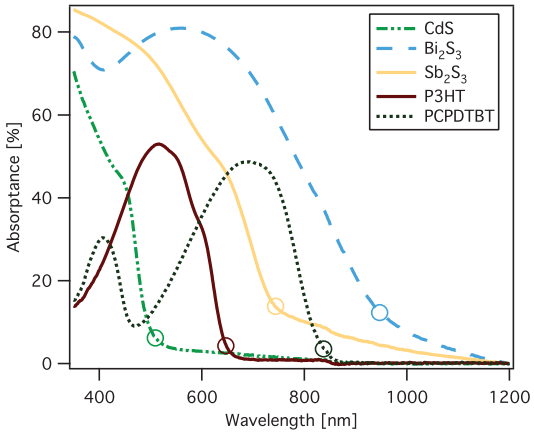

Fig. 2 Absorptance spectra of the different sulfides and polymers. The circles mark the estimated onsets.

Figure 4(a) displays the metal core levels for the different sulfide samples. For the Sb_2S_3 sample, the Sb $3d_{5/2}$ is overlapping with the O 1s core level from the TiO_2 substrate. From the Sb $3d_{3/2}$ level it is possible to distinguish two different contributions, indicating some degree of oxididation of the sulfide[39]. This is not surprising since the samples were exposed to air between preparation and the PES measurements, and Sb_2S_3 is known to oxidize easily in air[11,40,41]. However, we can't exclude an oxidation induced by the TiO_2 substrate. The curve fit in figure 4(a) is optimized using the Sb $3d_{3/2}$ line, giving the sulphide contribution to Sb $3d_{3/2}$ a binding energy of 539.5 eV. The split to the Sb$3d_{5/2}$ is fixed to 9.35 eV, consistent with earlier findings for both antimony sulfide and oxide[42,43]. The intensity of the Sb $3d_{3/2}$ is set to be two thirds of Sb $3d_{5/2}$. The O 1s from the TiO_2 substrate is also used in the curve fit and is intensity scaled relative the Ti 2p core level. The resulting O 1s contribution from the antimony oxide has a reasonable intensity compared to the corresponding Sb 3d (where the O/Sb ratio is 2 when including the differences in photoionisation cross section, see below).

As seen for measurements on CdS samples in figure 4(b), the Cd 3d core level shows one symmetric peak doublet with a binding energy of the Cd $3d_{5/2}$ peak at 405.7 eV and a spin-orbit split of 6.8 eV. No oxidation of Cd can be detected. In the Bi_2S_3 sample, the Bi 4f core level partly overlaps with the S 2p core level, as seen in figure 4(c). The binding energy of the main Bi $4f_{7/2}$ line is 158.8 eV with a spin orbit split of 5.3 eV to the Bi $4f_{5/2}$ line. There is also a second peak doublet at higher binding energy, which could indicate a small oxidation of bismuth[44].

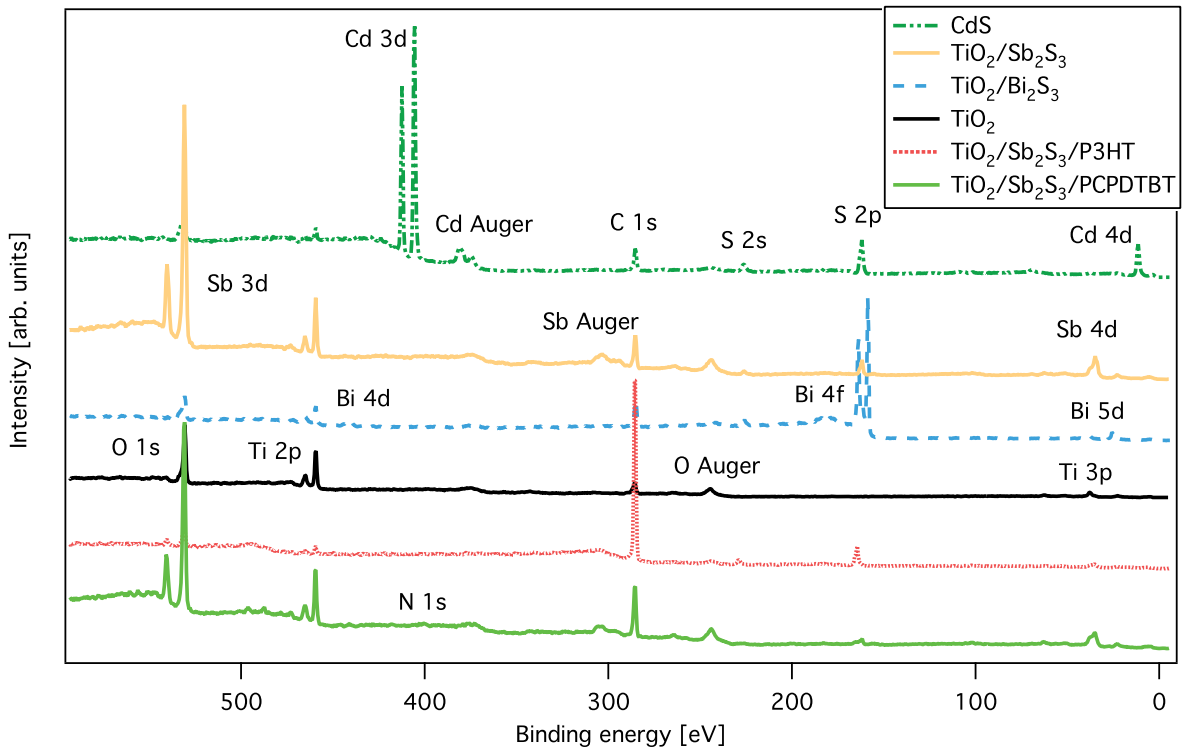

Fig. 3 Overview spectra of TiO_2, TiO_2/metal sulfides and TiO_2/metal sulfides/polymer measured with a photon energy of 758 eV. The spectra are shifted vertically for clarity.

Measurements of the S 2p core level from the different metal sulfides can be seen in figure 5. TiO_2/Sb_2S_3 shows one spin-orbit doublet with narrow peaks (FWHM=0.7 eV) indicating that all sulphur atoms are chemically equivalent in Sb_2S_3. For this sulfide the S $2p_{3/2}$ core level shows a binding energy of 161.93 eV and a spin-orbit split of 1.18 eV to the S $2p_{1/2}$ level. The S 2p core level peaks for TiO_2/CdS are slightly broader but have similar binding energies compared to TiO_2/Sb_2S_3. The S 2p in TiO_2/Bi_2S_3 is on the other hand shifted 0.4 eV towards lower binding energy.

If comparing the intensities of the metal core levels with the S 2p core level, it is possible to estimate the stoichiometry of the sulfides. Such calculations includes the photoionisation cross section and the assymetry parameters of the different core levels for the particular experimental configuration[45]. The compared spectra are measured using a photon energy of 758 eV. It is noted that this photon energy induces extra uncertainty of the stoichiometry estimations, due to a rather different kinetic energy, and in turn probe depth, of the photoelectrons from the sulfur compared to the metallic core levels in some cases. For Sb_2S_3, the Sb 4d core level is used for stoichiometry esimations to avoid confusion induced by the overlapping Sb 3d and O1s core levels. The estimated stoichiometry in CdS agrees with the expected value. For Sb_2S_3 and Bi_2S_3, the oxidised contribution was removed from the calculations and for the remaining sulfide, the stoichiometry is found to be $Sb_2S_{2.8}$ and $Bi_2S_{2.4}$ respectively. For Sb_2S_3, this is in good agreement with the expected stoichiometry, while for Bi_2S_3, the calculation might indicate that the bismuth sulfide surface is sulphur deficient. The sulphur difficiency may be linked to the shift of the sulphur 2p level to lower binding energy.

Figure 6(a) shows the valence levels for the metal sulfide samples together with a pristine mesoporous TiO_2 electrode. All spectra in this figure are scaled in intensity using the Ti 3p core level. The different intensities of the valence spectra therefore reflect thickness variations of the metal sulfides on the TiO_2 substrate. TiO_2 has a broad feature between binding energies 3.2–7 eV and a sharper feature at 8 eV. The shape of the valence levels are different for the different sulfides, especially at the outermost levels below the TiO_2 valence band edge. Calculations for Sb_2S_3 show that the outermost valence regions are made up by interactions of S 3p and Sb 5s orbitals[46]. The corresponding region in CdS are mainly S 3p and Cd 5p orbitals[47] and for Bi_2S_3, the valence levels consists of S 3p and Bi 6p orbitals[34].

It can be mentioned that the metal character of the outermost valence levels of the metal sulfides would be more easily

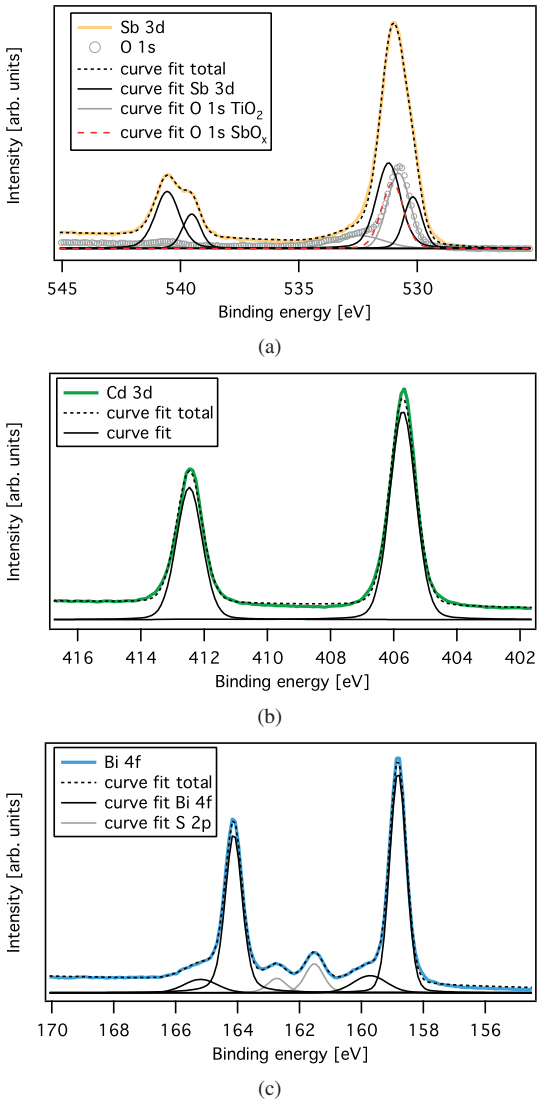

Fig. 4 The metal core levels on the TiO_2/sulfide samples measured with a photon energy of 758 eV. (a) The Sb 3d and O 1s core levels on the TiO_2/Sb_2S_3 and TiO_2 samples. The two signals are scaled in intensity relative the Ti 2p core level. The total curve fit includes all O 1s and Sb 3d peak fits. (b) The Cd 3d core level. (c) The Bi 4f and also the S 2p core levels.

accessible with higher photon energies[21], because of a higher relative photoionisation cross section for metals when measured with a higher photon energy. For the organic hole conductors on the other hand, the highest occupied levels are more easily detected with lower photon energies. Since the aim here is to measure and understand the complete interface, results with a lower photon energy are presented. Measurements with a higher photon energy (454 and 758 eV) show however very similar valence band edge positions and energy level alignment for the metal sulfides, as exemplified by Sb_2S_3 in figure 6(b).

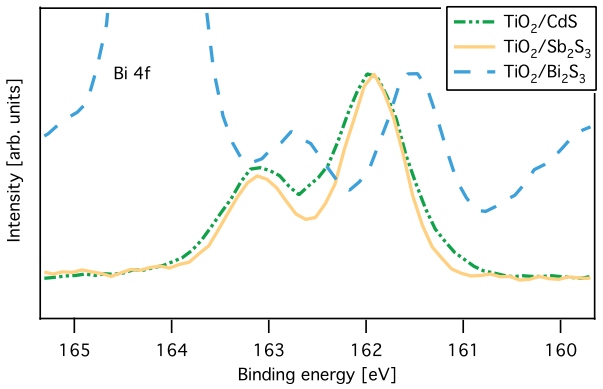

Fig. 5 The S 2p core level on the TiO_2/sulphide samples measured with a photon energy of 758 eV.

For pure TiO_2 there are occupied states below the valence band edge, which can be due to defects on the surface. When a sulfide is deposited onto TiO_2, these band gap states disappears, see figure 6(c). The same effect has earlier been observed when adsorbing dye molecules on mesoporous TiO_2[48].

3.2.1.1 Energy level alignment in TiO_2/metal sulfide interfaces. The driving force for eletron injection from the sulfide to TiO_2 is determined by the energy level alignment. The inset in figure 6(a) shows a close-up of the valence band edges. The oxidation seen in antimony and bismuth samples is not expected to influence the observed structures close to the valence band edges since oxides in general have a valence band edge at higher binding energy compared to sulfides[44]. It is clear that TiO_2 has the highest binding energy of the valence band edge, followed by CdS, Sb_2S_3 and Bi_2S_3 in order of decreasing binding energy. The energy of the valence band edge is estimated by the intersection of the linearly extrapolated experimental spectra with the baseline as shown in the inset figure. Using this method, the energy difference of the valence band edges between TiO_2 and the sulfides are found to be 1.2 eV for CdS, 1.8 eV for Sb_2S_3 and 1.9 eV for Bi_2S_3 (where the estimated error bars are 0.1 eV). Compared to reported bulk values, the value obtained here is similar for CdS but smaller for Sb_2S_3 where a distance of 2.0 eV is reported[15]. The energy level alignment is illustrated in figure 7 where the optical band gaps of TiO_2[49] and the metal sulfides (from figure 2) are used to draw the conduction band edges. According to this representation, CdS and Sb_2S_3 have a small driving force of about 0.4 eV for CdS and 0.3 for Sb_2S_3 for electron injection into TiO_2, while there is none with Bi_2S_3. Although these numbers contain the uncertainties discussed above, they give a good approximation of the energy level representation and are thus still useful for understanding device function.

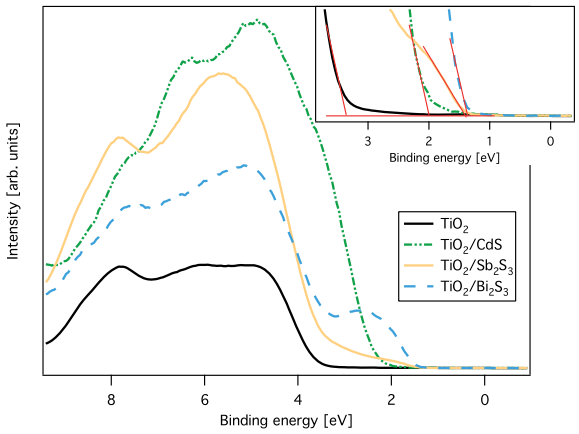

(a)

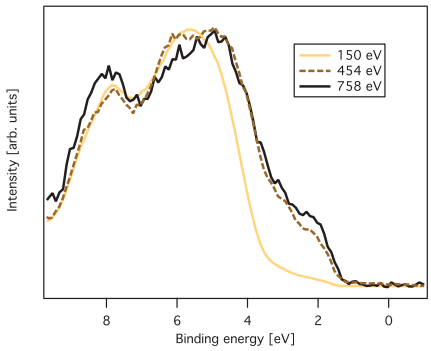

(b)

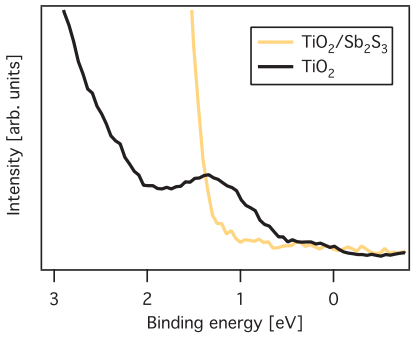

(c)

Fig. 6 (a) The valence levels on the TiO_2 and TiO_2/sulphide samples measured with a photon energy of 150 eV. Inset shows a close-up of the valence band edges. (b) The valence region of TiO_2/Sb_2S_3 measured with different photon energies. (c) A more detailed close-up on the band gap region in the TiO_2 and TiO_2/Sb_2S_3 samples measured with a photon energy of 150 eV.

3.2.2 TiO_2/Sb_2S_3/polymer interfaces. The overview spectra of the TiO_2/Sb_2S_3/polymer samples can be seen in figure 3. Carbon and sulphur is found in both polymers while nitrogen is only visible in PCPDTBT, in agreement with the molecular structures (see figure 1).

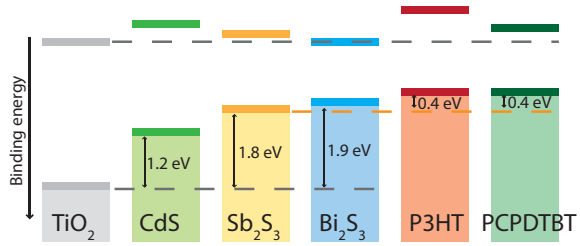

Fig. 7 The energy level alignment between TiO_2, the metal sulfides and polymers. The arrows indicate the measured binding energy differences of the valence band edges. Optical band gaps for the metal sulfides are estimated from absorptance measurements. For TiO_2, an optical bandgap of 3.2 eV is used[49].

As seen in figure 8 the sulphur in the polymers are clearly distinguishable from the sulphur in Sb_2S_3 due to a higher binding energy. The S 2p spin doublet in P3HT, originating from a thiophene unit, show a binding energy of 164.5 eV. This gives a shift of 2.6 eV to the S 2p in Sb_2S_3, similar to what has been observed for the S 2p core level in mixtures of CdS quantum dots/P3HT nanowires[35]. Each monomer unit in the PCPDTBT polymer contains three sulphur atoms, two in thiophene units (with C-S-C bonds) and one in a benzothiadiazole unit (with N-S-N bonds). The S 2p in the thiophene units in PCPDTBT have a very similar binding energy as the corresponding sulphur in P3HT and as in earlier reported studies[50]. The higher binding energy contribution to the sulphur signal from PCPDTBT originates from the benzothiadiazole unit. The S 2p peaks from the polymers are broader when the polymer is deposited onto Sb_2S_3 compared to ITO. This could indicate a small interaction between the polymer and the sulfide. Note that the intensity of the S 2p originating from Sb_2S_3, observed at 162 eV, is barely visible for the TiO_2/Sb_2S_3/P3HT sample indicating that a thick polymer film is shielding the sulfide film. The inset therefore shows this sample mesured with a higher photon energy where the measurement is more bulk sensitive and the S 2p from Sb_2S_3 is more visible.

Figure 9 displays the valence levels of the TiO_2/Sb_2S_3, TiO_2/Sb_2S_3/polymer and ITO/polymer samples. The overall valence structure of the TiO_2/Sb_2S_3/PCPDTBT sample is similar to TiO_2/Sb_2S_3. The TiO_2/Sb_2S_3/P3HT shows on the other hand similar structure of the valence levels as ITO/P3HT. Both these findings can be explained by a thicker organic film on the TiO_2/Sb_2S_3/P3HT sample than on the TiO_2/Sb_2S_3/PCPDTBT sample. A reason for the different thicknesses of the two polymers could be the difference in molecular weight of the two polymers (see experimental). Due to the different thicknesses of the polymer over-standing layer, the spectra in figure 9 are intensity normalized to the highest peak and not via the Ti 3p core level.

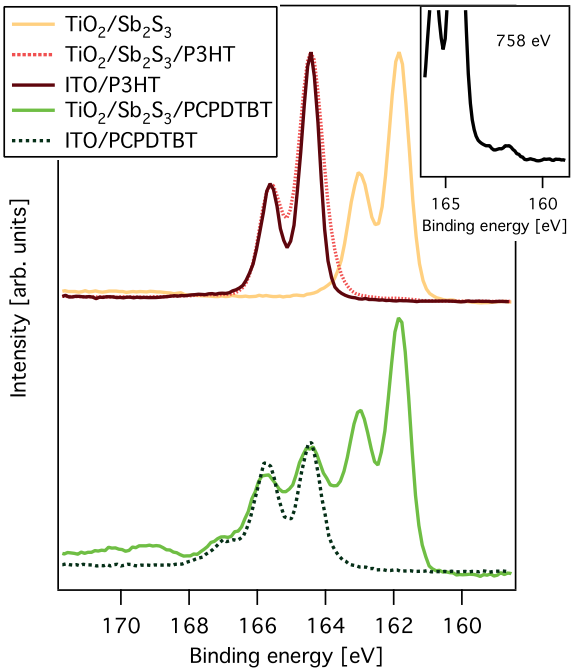

Fig. 8 The S 2p core levels on the TiO_2/Sb_2S_3, TiO_2/Sb_2S_3/polymer and ITO/polymer samples measured with a photon energy of 454 eV. Inset shows close-up of the sulfide contribution of the TiO_2/Sb_2S_3/P3HT sample measured with a photon energy of 758 eV.

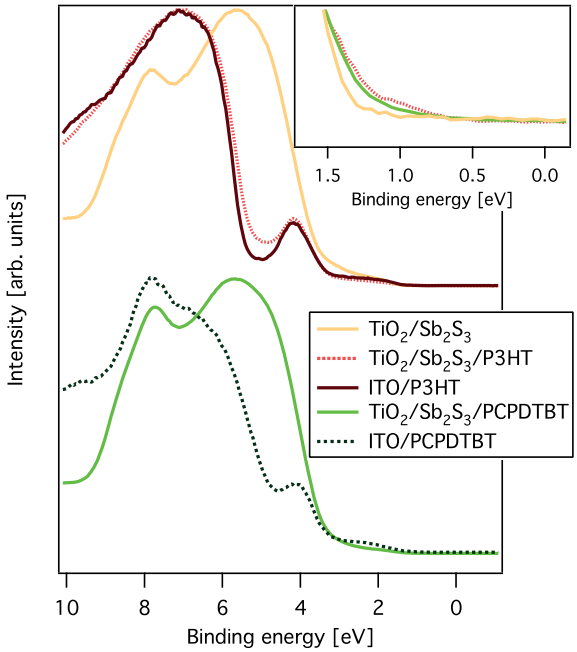

Fig. 9 The valence levels of the TiO_2/Sb_2S_3, TiO_2/Sb_2S_3/polymer and ITO/polymer samples measured with a photon energy of 150 eV. Inset shows the valence band edges of the TiO_2/Sb_2S_3 and TiO_2/Sb_2S_3/polymer samples.

For the ITO/polymer samples, the binding energy region between 0–4 eV shows similar structure. In P3HT the peak at a binding energy of 3.5 eV is assigned to localised π-bands and the region between 0–2.5 eV are delocalised π-bands[51,52]. The highest occupied levels in PCPDTBT has also been assigned to the conjugated π-system that is delocalised over the thiopene and benzene units[38,53].

3.2.2.1 Energy level alignment in TiO_2/Sb_2S_3/polymer interfaces. The energy distance of the valence band edges of the metal sulfide and the polymer is the driving force for charge separation when the holes move from Sb_2S_3 to the polymer in the solar cell. The inset in figure 9 shows a close up on the edges of the TiO_2/Sb_2S_3 and TiO_2/Sb_2S_3/polymer samples. Here we can see that the valence band edges of the polymers are at lower binding energy compared to Sb_2S_3. This indicates that even though the PCPDTBT film is very thin the outermost valence levels are clearly observed. The valence band edges are separated approximately 0.4 eV between Sb_2S_3 and the polymers. This is a sufficient driving force for the charge separation process in a solar cell, see figure 7. Comparing these values to the valence band edge position found for the different metal sulfides in the inset in figure 6(a), the metal sulfide–polymer energy difference can be expected to be 1.0 eV for CdS and 0.3 eV for Bi_2S_3.

3.3 Solar cell characterization

To further investigate the functional effects of differences in energy level alignments for the material combinations synthesized here, solar cell devices were built and tested using the different sulfides on TiO_2 and P3HT as hole transporting material. PCPDTBT is not included in the device characterization as the thin polymer layers led to short-circuiting of devices and therefore made it difficult to assess the performance of the TiO_2/sulfide/polymer interfaces. However, an IPCE spectrum of a TiO2/Sb_2S_3/PCPDTBT is included for comparison.

Figure 10(a) shows representative IV-curves under 1 sun illumination and in the dark for devices with the different metal sulfides. Parameters extracted from the measurements are found in table 1. Solar cells including Sb_2S_3 show the highest short circuit current (J_{sc}=9.48 mA cm^{-2}) and fill factor (FF=0.52) giving the highest efficiency in this comparison (η=3.35%). Even though solar cells with CdS show a high open circuit voltage (V_{oc}=0.79V) the short circuit current is low (J_{sc}=1.27 mA cm^{-2}) resulting in a lower efficiency (η=0.46%). Bi_2S_3 give solar cells with low current and voltage and therefore also a low efficiency (η=0.02%). While Bi_2S_3 seems to be quite conductive in both forward and reverse bias, there is limited photocurrent generation.

In order to determine where the short-circuit current was being generated in the devices, IPCE spectra were also mea-

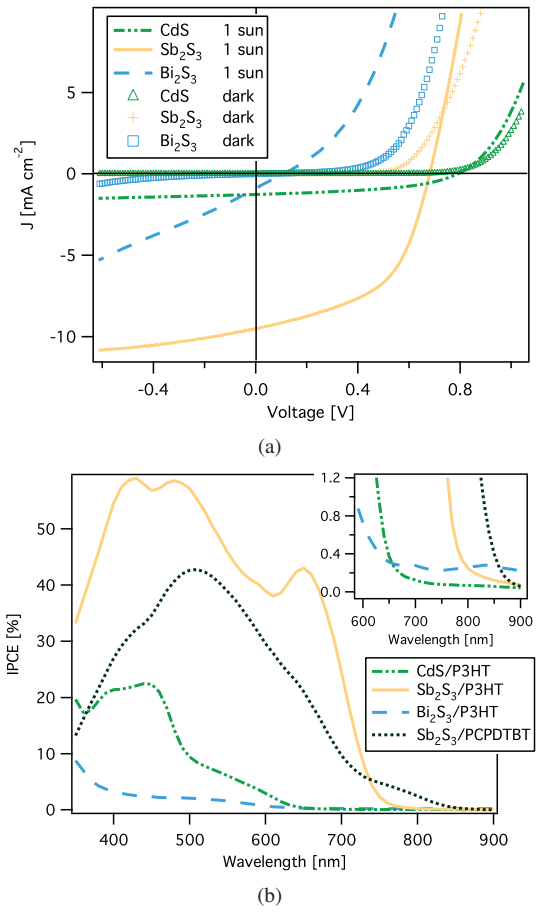

Fig. 10 (a) IV and dark curves of solar cells of the architecture TiO_2(bl)/TiO_2(np)/sulfide/P3HT/silver. (b) IPCE spectra of the same solar cells as in (a). The inset shows a close up of the near infrared region.

sured and are shown in figure 10(b). The short circuit currents predicted from the IPCE measurements are in good agreement with the IV measurements, see table 1. From the spectra, it can be seen that for CdS cells the highest IPCE is achieved through excitation of the cadmium sulfide but that some current is also generated through excitation of the P3HT. It is clear however, that the current is limited by the large bandgap of CdS. The IPCE spectrum of the Sb_2S_3/P3HT solar cell matches the broad absorption spectrum of antimony sulfide with an IPCE onset beyond 750 nm. Whether the P3HT contributes to the photocurrent is unclear from this spectrum. However, the IPCE spectrum of a TiO_2/Sb_2S_3/PCPDTBT solar cell shows photocurrent generation beyond 750 nm, indicating a small contribution of the polymer to the photocurrent. Finally, the IPCE of the bismuth sulfide solar cell is highest where P3HT absorbs. A close-up of the near infrared region of the IPCE is displayed in the inset in figure 10(b) and reveals a very limited

Table 1 IV parameters and J_{sc} predicted from IPCE measurements.

Parameters	CdS	Sb_2S_3	Bi_2S_3
J_{sc} [mA cm^{-2}]	1.27	9.48	0.89
V_{oc} [V]	0.79	0.68	0.11
FF	0.46	0.52	0.24
η [%]	0.46	3.35	0.02
J_{sc} [mA cm^{-2}] IPCE	1.59	9.65	0.33

amount of current generation from the bismuth sulfide itself at wavelengths longer than the absorption onset of P3HT.

3.3.1 Effects of the energy level alignment. The solar cell characteristics described in the previous section is here related to the results from the photoelectron spectroscopy measurements. According to the energy level alignment in figure 7 both CdS and Sb_2S_3 should have sufficient driving force for electron injection into TiO_2. In addition Sb_2S_3 also has a favourable distance between the valence band edge of Sb_2S_3 and the HOMO of both P3HT and PCPDTBT giving sufficient driving force for regeneration of the metal sulfide. In this sense, Sb_2S_3 is a good choice as a light absorber in TiO_2/metal sulfide/polymer configurations as energy losses at the interface are minimized, which is also indicated by the high efficiency of Sb_2S_3 devices, both in this work and other studies[5].

The low current of devices with CdS indicates that the TiO_2/CdS/P3HT is not an optimized structure for CdS devices, as high currents[28,54] and good hole transfer have been observed in blends of CdS/P3HT[55].

Even though Bi_2S_3 show high absorption, the current produced in the Bi_2S_3 devices mainly originates from absorption in P3HT. This could be explained by the unfavourable energy level alignment between the Bi_2S_3 and TiO_2 conduction band edges with no or very low driving force for electron injection, in agreement with an earlier study[56]. To enhance electron injection, the conduction band edge should be shifted to lower binding energies by, for example, forming a dipole layer at the interface, using *e.g.* sulphur ions[56]. Other reasons for the low performance of solar cells with Bi_2S_3 could be related to the sulphur deficiency observed in this material.

The current generation from excitations of the polymers observed in IPCE spectra could either come from electron transfer to a sulfide or directly to the TiO_2. It is clear from the energy alignment that P3HT has sufficient driving force for electron transfer to either the sulfides or to TiO_2. PCPDTBT has sufficient driving force for electron transfer to TiO_2 and is likely to have driving force for electron transfer to Sb_2S_3 also. It should however be noted that for both CdS and Sb_2S_3 charge generation from the sulfide appears more efficient than charge generation from the polymer. It is likely that charge generation from polymers is limited by exciton diffusion to a TiO_2/sulfide interface[55].

Finally, the devices show an increasing open-circuit voltage and decreasing dark current with increasing bandgap of the metal sulfide. As the open-circuit voltage is not directly related to the valence and conduction band positions of the sulfides but to the Fermi level in TiO_2 and the HOMO level of the polymer, this could reflect a suppression of the back reaction at the TiO_2/sulfide/polymer interface, as the sulfide band gap is increased.

4 Conclusions

We have demonstrated that photoelectron spectroscopy can be used to determine the electronic structure and energy level alignment of TiO_2/metal sulfide and complete TiO_2/Sb_2S_3/polymer interfaces. The obtained alignments correlate well with the function of solar cells including the different metal sulfides.

Devices utilising Sb_2S_3 gave the highest conversion efficiencies in this comparison which is explained by the most favourable energy level alignment for both electron injection into TiO_2 and hole injection into the polymer.

In contrast, Bi_2S_3 sensitised systems show unfavourable energy level alignment for electron injection into TiO_2. As a consequence, devices including Bi_2S_3 show low efficiency and it could be seen that the generated current comes from absorption in the polymer rather than Bi_2S_3.

Devices with CdS as light absorber show a performance in between that of Sb_2S_3 and Bi_2S_3. The generated current is expected to come both from the sulfide and the polymer, but is ultimately limited by the large bandgap of CdS.

As a method for determining energy level alignment, photoelectron spectroscopy offers the possibility for studying complete interfaces in the actual device geometry. In addition, this method reveals information about the detailed electronic structure of the materials involved, which enables detailed characterization of the interfaces.

Acknowledgements

This work was supported by the Swedish Energy Agency, by the Göran Gustafsson Foundation, by the Carl Trygger Foundation, by StandUp for energy, by the Swedish Research Council (2012-4721), by a Marie Curie Intra-European Fellowship within the seventh European Community Framework Programme, by the Engineering and Physical Science Research Council (EPSRC) through the Supergen (EP/G031088/1) and UK–India (EP/H040218/2) programmes, by the Royal Society and by the European Community's Seventh Framework Programme (NanoMatcell, grant agreement no. 308997). We acknowledge MAX-IV for support during measurements.

References

1 G. Hodes and D. Cahen, *Accounts of Chemical Research*, 2012, **45**, 705–713.
2 A. Hagfeldt, G. Boschloo, L. Sun, L. Kloo and H. Pettersson, *Chem. Rev.*, 2010, **110**, 6595–6663.
3 M. Grätzel, *Nature*, 2001, **414**, 338–344.
4 S.-J. Moon, Y. Itzhaik, J.-H. Yum, S. M. Zakeeruddin, G. Hodes and M. Grätzel, *The Journal of Physical Chemistry Letters*, 2010, **1**, 1524–1527.
5 J. A. Chang, J. H. Rhee, S. H. Im, Y. H. Lee, H.-j. Kim, S. I. Seok, M. K. Nazeeruddin and M. Grätzel, *Nano Letters*, 2010, **10**, 2609–2612.
6 S. H. Im, C.-S. Lim, J. A. Chang, Y. H. Lee, N. Maiti, H.-J. Kim, M. K. Nazeeruddin, M. Grtzel and S. I. Seok, *Nano Letters*, 2011, **11**, 4789–4793.
7 F. T. F. O'Mahony, T. Lutz, N. Guijarro, R. Gomez and S. A. Haque, *Energy Environ. Sci.*, 2012, **5**, 9760–9764.
8 R. Vogel, P. Hoyer and H. Weller, *The Journal of Physical Chemistry*, 1994, **98**, 3183–3188.
9 L. Etgar, P. Gao, Z. Xue, Q. Peng, A. K. Chandiran, B. Liu, M. K. Nazeeruddin and M. Graetzel, *J. Am. Chem. Soc.*, 2012, **134**, 17396–17399.
10 H. C. Leventis, F. OMahony, J. Akhtar, M. Afzaal, P. OBrien and S. A. Haque, *Journal of the American Chemical Society*, 2010, **132**, 2743–2750.
11 Y. C. Choi, D. U. Lee, J. H. Noh, E. K. Kim and S. I. Seok, *Advanced Functional Materials*, 2014, doi:10.1002/adfm.201304238.
12 H. Ohkita, S. Cook, Y. Astuti, W. Duffy, S. Tierney, W. Zhang, M. Heeney, I. McCulloch, J. Nelson, D. D. C. Bradley and J. R. Durrant, *Journal of the American Chemical Society*, 2008, **130**, 3030–3042.
13 C. Karthikeyan, H. Wietasch and M. Thelakkat, *Advanced Materials*, 2007, **19**, 1091–1095.
14 Y. Xu and M. Schoonen, *American Mineralogist*, 2000, **85**, 543–556.
15 J. H. Rhee, C.-C. Chung and E. W.-G. Diau, *NPG Asia Materials*, 2013, **5**, e68.
16 Y.-L. Lee and Y.-S. Lo, *Advanced Functional Materials*, 2009, **19**, 604–609.
17 H. Lee, H. C. Leventis, S.-J. Moon, P. Chen, S. Ito, S. A. Haque, T. Torres, F. Nesch, T. Geiger, S. M. Zakeeruddin, M. Grätzel and M. K. Nazeeruddin, *Advanced Functional Materials*, 2009, **19**, 2735–2742.
18 N. Guijarro, T. Lutz, T. Lana-Villarreal, F. O'Mahony, R. Gómez and S. A. Haque, *The Journal of Physical Chemistry Letters*, 2012, **3**, 1351–1356.
19 H. Ishii, K. Sugiyama, E. Ito and K. Seki, *Advanced Materials*, 1999, **11**, 605–625.
20 Q. Chen, B. J. Worfolk, T. C. Hauger, U. Al-Atar, K. D. Harris and J. M. Buriak, *ACS Applied Materials and Interfaces*, 2011, **3**, 3962–3970.
21 R. Lindblad, D. Bi, B.-w. Park, J. Oscarsson, M. Gorgoi, H. Siegbahn, M. Odelius, E. M. J. Johansson and H. Rensmo, *The Journal of Physical Chemistry Letters*, 2014, 648–653.
22 E. Edri, H. Cohen and G. Hodes, *ACS Applied Materials and Interfaces*, 2013, **5**, 5156–5164.
23 E. Johansson, R. Schölin, H. Siegbahn, A. Hagfeldt and H. Rensmo, *Chem. Phys. Lett.*, 2011, **515**, 146–150.
24 J. Boucle, P. Ravirajan and J. Nelson, *J. Mater. Chem.*, 2007, **17**, 3141–3153.
25 E. M. J. Johansson, R. Lindblad, H. Siegbahn, A. Hagfeldt and H. Rensmo, *ChemPhysChem*, 2014, **15**, 1006–1017.
26 T. Lutz, A. MacLachlan, A. Sudlow, J. Nelson, M. S. Hill, K. C. Molloy and S. A. Haque, *Phys. Chem. Chem. Phys.*, 2012, **14**, 16192–16196.
27 H. C. Leventis, S. P. King, A. Sudlow, M. S. Hill, K. C. Molloy and S. A. Haque, *Nano Letters*, 2010, **10**, 1253–1258.
28 S. Dowland, T. Lutz, A. Ward, S. P. King, A. Sudlow, M. S. Hill, K. C.

Molloy and S. A. Haque, *Advanced Materials*, 2011, **23**, 2739–2744.
29 N. Bansal, F. T. F. O'Mahony, T. Lutz and S. A. Haque, *Adv. Energy Mater.*, 2013, **3**, 986–990.
30 F. T. F. O'Mahony, U. B. Cappel, N. Tokmoldin, T. Lutz, R. Lindblad, H. Rensmo and S. A. Haque, *Angewandte Chemie International Edition*, 2013, **52**, 12047–12051.
31 M. Bassler, J. O. Forsell, O. Björneholm, R. Feifel, M. Jurvansuu, S. Aksela, S. Sundin, S. L. Sorensen, R. Nyholm, A. Ausmees and *et al*, *J. Electron Spectrosc.*, 1999, **101–103**, 953.
32 M. Y. Versavel and J. A. Haber, *Thin Solid Films*, 2007, **515**, 7171 – 7176.
33 N. Yesugade, C. Lokhande and C. Bhosale, *Thin Solid Films*, 1995, **263**, 145 – 149.
34 J. Grigas, E. Talik and V. Lazauskas, *physica status solidi (b)*, 2002, **232**, 220–230.
35 S. Ren, L.-Y. Chang, S.-K. Lim, J. Zhao, M. Smith, N. Zhao, V. Bulović, M. Bawendi and S. Gradečak, *Nano Letters*, 2011, **11**, 3998–4002.
36 W. C. Tsoi, S. J. Spencer, L. Yang, A. M. Ballantyne, P. G. Nicholson, A. Turnbull, A. G. Shard, C. E. Murphy, D. D. C. Bradley, J. Nelson and J.-S. Kim, *Macromolecules*, 2011, **44**, 2944–2952.
37 J.-H. Im, J. Chung, S.-J. Kim and N.-G. Park, *Nanoscale Res. Lett.*, 2012, **7**, 353.
38 G. L. Gibson, T. M. McCormick and D. S. Seferos, *Journal of the American Chemical Society*, 2012, **134**, 539–547.
39 T. Birchall, J. A. Connor and L. H. Hillier, *J. Chem. Soc., Dalton Trans.*, 1975, 2003–2006.
40 B. Reeja-Jayan and A. Manthiram, *RSC Adv.*, 2013, **3**, 5412–5421.
41 N. Maiti, S. H. Im, C.-S. Lim and S. I. Seok, *Dalton Trans.*, 2012, **41**, 11569–11572.
42 V. Zakaznova-Herzog, S. Harmer, H. Nesbitt, G. Bancroft, R. Flemming and A. Pratt, *Surface Science*, 2006, **600**, 348 – 356.
43 R. Reiche, D. Dobler, J. Holgado, A. Barranco, A. Martn-Concepcin, F. Yubero, J. Espins and A. Gonzlez-Elipe, *Surface Science*, 2003, **537**, 228 – 240.
44 T. P. Debies and J. Rabalais, *Chemical Physics*, 1977, **20**, 277 – 283.
45 J. Yeh and I. Lindau, *Atom. Data Nucl. Data*, 1985, **32**, 1 – 155.
46 P. E. Lippens and et al., *Phys. Rev. B*, 1997, **56**, 13054–13065.
47 P. Schröer, P. Krüger and J. Pollmann, *Phys. Rev. B*, 1994, **49**, 17092–17101.
48 U. B. Cappel, S. Plogmaker, E. M. J. Johansson, A. Hagfeldt, G. Boschloo and H. Rensmo, *Phys. Chem. Chem. Phys.*, 2011, **13**, 14767–14774.
49 H. Lin, C. Huang, W. Li, C. Ni, S. I. Shah and Y.-H. Tseng, *Appl. Catal. B-Environ.*, 2006, **68**, 1 – 11.
50 U. Aygl, H. Peisert, J. Frisch, A. Vollmer, N. Koch and T. Chass, *ChemPhysChem*, 2011, **12**, 2345–2351.
51 W. R. Salaneck and et al, *J. Chem. Phys.*, 1988, **89**, 4613–4619.
52 J. Frisch, A. Vollmer, J. Rabe and N. Koch, *Org. Electron.*, 2011, **12**, 916 – 922.
53 H. Hintz, H. Peisert, U. Aygl, F. Latteyer, I. Biswas, P. Nagel, M. Merz, S. Schuppler, D. Breusov, S. Allard, U. Scherf and T. Chass, *ChemPhysChem*, 2010, **11**, 269–275.
54 S. A. Dowland, L. X. Reynolds, A. MacLachlan, U. B. Cappel and S. A. Haque, *J. Mater. Chem. A*, 2013, **1**, 13896–13901.
55 U. B. Cappel, S. A. Dowland, L. X. Reynolds, S. Dimitrov and S. A. Haque, *The Journal of Physical Chemistry Letters*, 2013, **4**, 4253–4257.
56 L. M. Peter, K. G. U. Wijayantha, D. J. Riley and J. P. Waggett, *The Journal of Physical Chemistry B*, 2003, **107**, 8378–8381.

Table of contents entry

The experimental energy level alignment has been determined for complete TiO_2/metal sulfide/polymer interfaces using photoelectron spectroscopy and the results are compared to the function of solar cells.

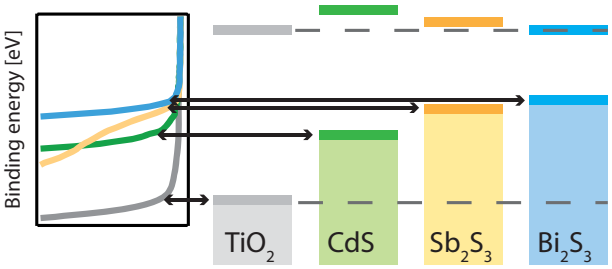

Fig. 11 Table of contents graphic.